VATT Optical Performance During 98 Oct as Measured with an Interferometric Hartmann Wavefront Sensor

S. C. West, D. Fisher
Multiple Mirror Telescope Observatory

M. Nelson
Vatican Advanced Technology Telescope

MMTO Internal Technical Memo #00-01, Oct. 2000

Abstract

During 98 Oct, we made measurements of the optical performance of the VATT using an interferometric Hartmann wavefront sensor. Recently, the MMTO has produced a new software suite to analyze optical performance and correct mirror figure using this type of instrument. We decided to test-pilot the software with this VATT data. It seems appropriate to present some of the results as an archive of the optical performance of the VATT in late 1998. The pupil aberrations and diffraction psfs were obtained from time-averaged data minimizing the contributions of seeing effects on the telescope optics. The memo is not meant to be an exhaustive analysis of this wavefront sensor data.

I. Instrumental Setup

A wavefront sensor for the VATT was designed to use the interferometric technique developed at the Nordic Optical Telescope by Tapio Korhonen [1-3]. Our device (shown in Figure 1) provides 29 apertures across the VATT primary mirror. The telescope beam is collimated and a pupil is imaged onto a Hartmann mask. A converging lens images a matrix of spots onto a CCD formed by the interference of adjacent Hartmann apertures. The bandpass is defined by a 710nm blue cut-off filter and the near infrared response of the CCD (a 512 x 512 Apogee KX-260). The camera control software runs under Linux (“Camera” written by Elwood Downey). The instrument is shown attached to the VATT in Figure 2.

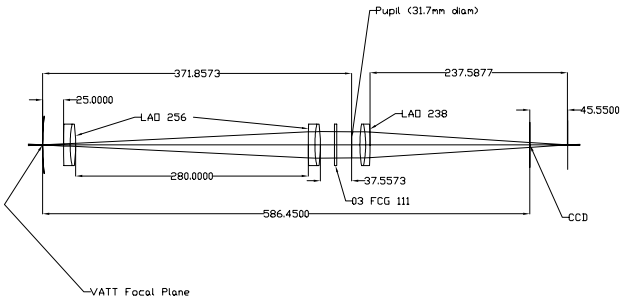

Figure 1: Schematic of the VATT wavefront sensor.

Figure 2: The interferometric Hartmann wavefront sensor attached to the VATT.

II. Data Reduction

The data reduction software was recently written for the MMTO and will be described elsewhere. Briefly though, an aberration-free system will produce an interferogram with an exactly square pattern. Each interference spot is formed by 4 apertures in the Hartmann mask. If the phase in each of these apertures is identical, the m=0 interference will be centered exactly between the apertures. Any phase difference among apertures causes spot motion away from the center position.

The software analyzes systematic spot motions corresponding to Zernike pupil wavefront aberrations.

Typical time-averaged interferograms obtained at the telescope are shown in Figure 3. A diode laser reference produces

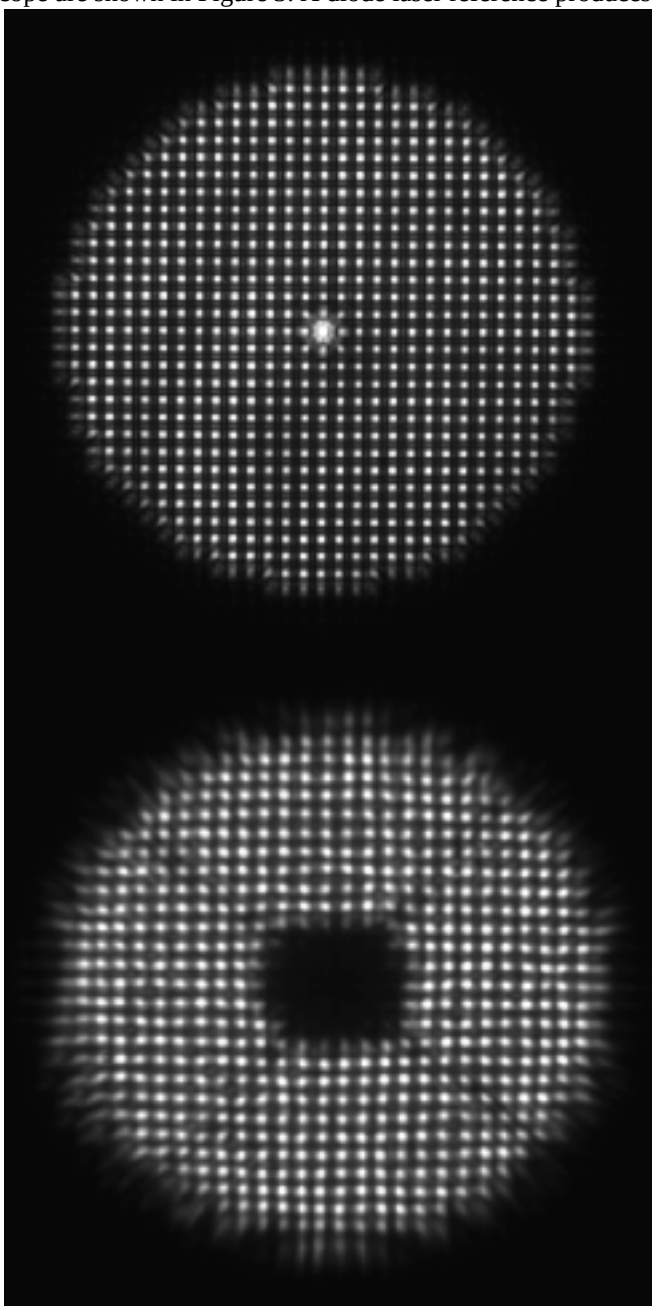

Figure 3: Interferograms of the laser reference source (top) and a typical time-averaged stellar source.

an interferogram containing the phase error distribution of the instrument (top figure). This is subtracted from the stellar interferogram (bottom figure) in order to remove instrumental effects from the telescope pupil aberrations.

After calculating the Zernike aberrations, the software uses the telescope geometry to construct a diffraction image psf of the telescope optics.

III. Results

A. Mis-collimation aberration coefficients

The secondary mirror was moved in known amounts, and the resulting low-order aberrations were measured with the instrument and compared to predictions calculated with the OSLO SIX optical design program. Inverting the results allows us to the collimate the telescope using the wavefront sensor as feedback.

Table 1 shows the sensitivity of Zernike defocus, third-order spherical, and coma to various motions of the secondary (M2). The coefficients correspond to the wavefront phase error at the edge of the pupil. The results are derived from the average sensitivity of many observations. The discrepancy between the predicted and observed coma coefficients may be due to improper calibration of the secondary linkage or to a scaling error in the data reduction geometry.

Table 1: Observed vs. predicted M2 mis-collimation terms

	defocus per piston nm/um	**spherical per piston nm/um**	**coma per decenter nm/um**	**coma per tip nm/arcsec**
predicted	31	1	8.5	15.2
observed	33	0.8	6	11

After deriving the misalignment coma with the wavefront sensor, these coefficients were used to null the coma to less than 20nm in one iteration of secondary correction. Figure 4 illustrates the usage of Table 1 coefficients in nulling the misalignment coma.

B. Elevation dependent aberrations

The collimation and mirror figure stability as a function of elevation angle were briefly investigated. The elevation axis was cycled 3 times from zenith to 20-deg in steps while leaving the optical geometry stationary. At each step, the wavefront errors were measured. Figure 5 shows the change in focus and spherical due to elevation. Overall, there was a change of approximately 1200 nm of defocus and 40 nm of spherical. According to Table 1, the ratio of defocus to spherical due to a despace error between M1 and M2 is 33 which is consistent with these data. This suggests that the spacing between M1 and M2 changes by about 35 microns over this interval.

The elevation-dependent coma is shown in Figure 6. There is highly repeatable hysteresis illustrating that the relative orientation of M2 depends not only upon elevation, but also upon the direction that the axis was moved. The total change in the

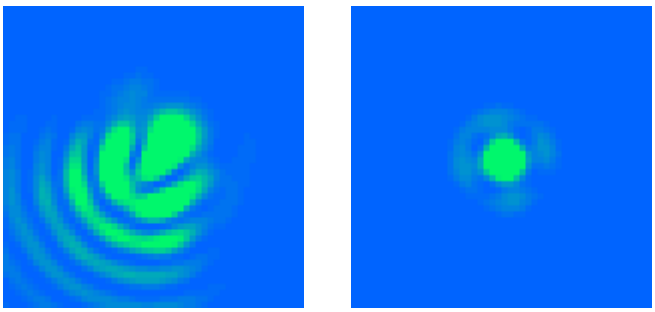

Figure 4: Diffraction images calculated from the measured wavefront aberrations. Each has defocus removed and is shown in a 1 arcsec square box. Left shows 400 nm of starting coma that was measured with the wavefront sensor. The coefficients in Table 1 were then used to update the position of the secondary. After remeasuring the wavefront aberrations, the resulting image (right) shows less than 20 nm of coma remaining. Still visible however are some static aberrations discussed later.

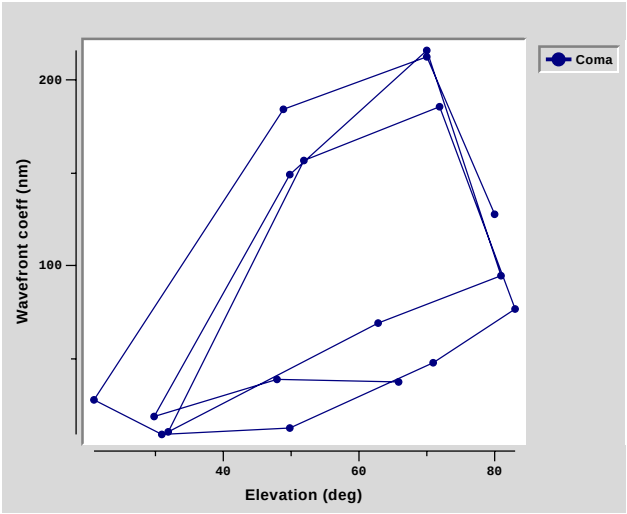

Figure 6: The elevation dependence of coma. The coma was nulled near 20-deg elevation prior to taking this data.

coma coefficient is about 200 nm (wavefront) which corresponds either to 18-arcsec of tilt or 30-microns of decenter or some combination. The angle remains nearly constant.

The elevation-dependent trefoil and fifth-order astigmatism are shown in Figure 7. Both errors are very small, and the angles of each remain constant vs. elevation. The trefoil suggests that the hardpoints are not significantly influencing the primary mirror figure.

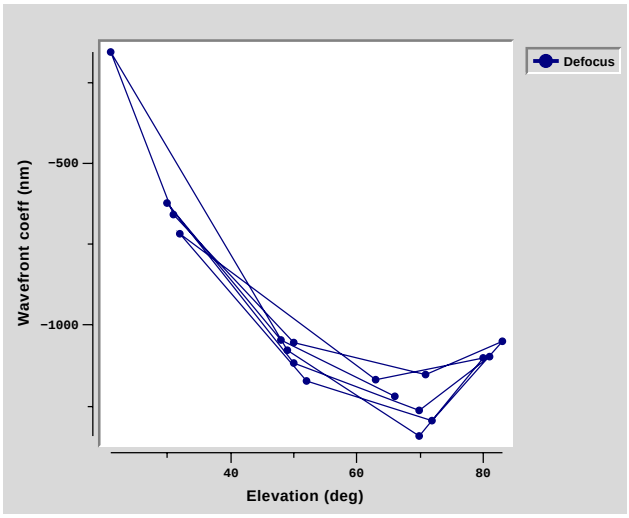

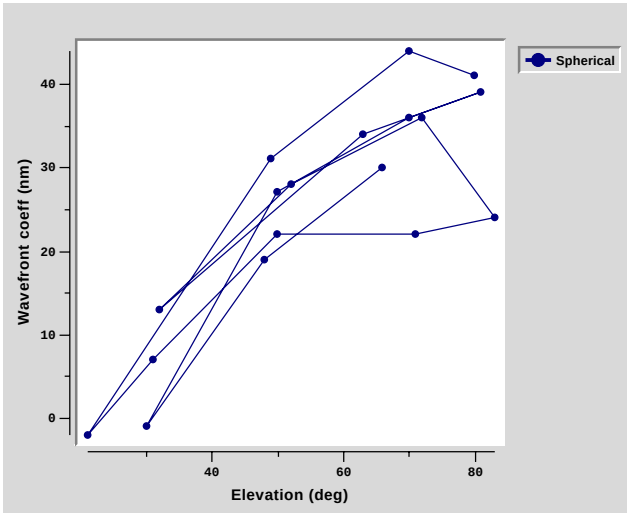

Figure 5: Elevation dependent wavefront defocus and third-order spherical. The variations are highly repeatable and suggest that the M1 to M2 spacing changes by about 35 microns.

The elevation-dependent astigmatism is shown in Figure 8. The magnitude varies by about 200nm (wavefront), and the angle remains constant. It's grows with elevation suggesting that its origin is in the axial support system of the primary mirror.

IV. Thermal Control vs. Spherical

The effectiveness of the primary mirror ventilation[4] in controlling third-order spherical aberration is illustrated in Figure 9. This time series is typical of the changes in spherical aberration we saw each night after the primary mirror thermal control system was started and suggests that the mirror ventilation brings the front and backplates of the mirror to a common temperature very well.

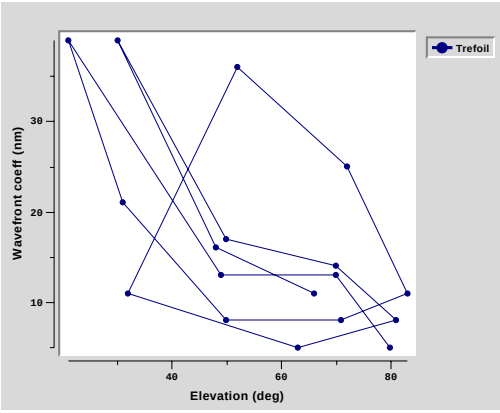

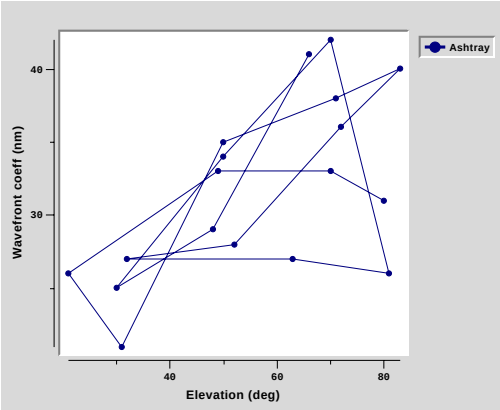

Figure 7: Elevation-dependent trefoil and 5th order astigmatism.

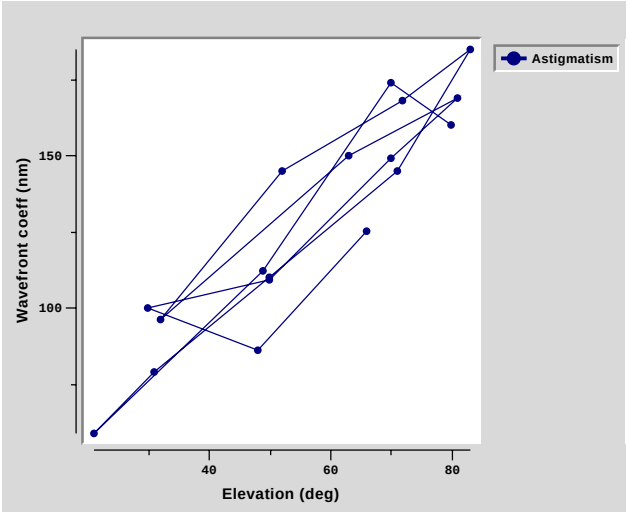

Figure 8: Elevation dependence of astigmatism shown for repeated elevation cycling.

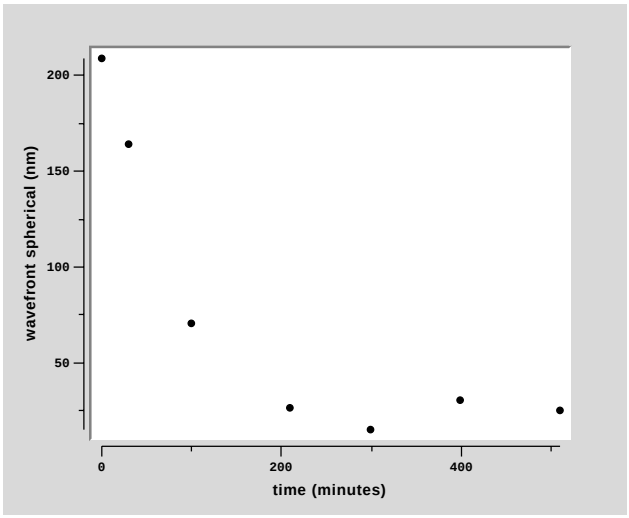

Figure 9: Spherical aberration is shown as a function of time from when the primary mirror thermal control system was turned on (t=0).

V. Conclusions

An interferometric Hartmann wavefront analyzer was attached to the VATT during Oct 98. We have briefly summarized some of these results in order to archive past telescope performance. Data reduction was accomplished with software recently written for the MMT. After seeing (and other sources of vibration) have been removed, the right image of Figure 4 is representative of the image quality the telescope was producing at that time which was quite good.

The elevation dependence of low-order aberrations are shown in detail. Their repeatabilities were ascertained by repeatedly cycling the elevation axis. Both 3rd and 5th order astigmatisms were functions of elevation and seem to be associated with the fraction of the mirror weight placed upon the axial support system. In each case, they are largest at zenith (with magnitudes of 200 and 40 nm wavefront amplitude respectively) and near zero at horizon. On the other hand, trefoil was near zero at zenith and increased to about 40nm at horizon.

Taken together, third order spherical and defocus changes provide strong evidence that the M1 to M2 spacing varied by about 35 microns from zenith to 20-deg elevation.

Coma exhibited over 200nm of elevation variation which corresponds to 18-arcsec of tilt or 30-microns of decenter (or some combination). In addition, it showed ~100nm of hysteresis so the M2 orientation depended upon elevation and the direction the axis was moved.

Finally, we showed the effectiveness of the primary mirror thermal ventilation system in removing spherical aberration caused by a non-uniform temperature distribution in the blank.

VI. References

[1] T. K. Korhonen, “Interferometric Method for Optical Testing and Wavefront Error Sensing,” *SPIE* **444**, 249-252 (1984).

[2] T. K. Korhonen, S. T. Haarala, J. O. Piironen, and A. K. Sillanpaa, “Interferometric Optical Test and Diffraction Based Image Analysis,” *SPIE* **628**, p. 486-491 (1986).

[3] T. Korhonen, T. Lappalainen, and A. Sillanpaa, “Hartmann Interferometric Testing of Large Mirrors,” *SPIE* **1531**, p. 44-49 (1991).

[4] S.C West, R. H Nagel, D. Harvey, A. Brar, B. Phillips, J. Ray, T.J. Trebisky, R. Cromwell, N.J. Woolf, C. Corbally, R. Boyle, D. Blanco, and L. Otten, “Progress at the Vatican Advanced Technology Telescope,” *Optical Telescopes of Today and Tomorrow*, Proc. SPIE **2871**, p. 74, ed. Arne Arnenberg, Hven Sweden.